Structure of human Fe-S assembly sub-complex reveals unexpected cysteine desulfurase architecture and acyl-ACP-ISD11 interactions

Supplementary Information

Seth A. Cory[a], Jonathan G. Van Vranken[b], Edward J. Brignole[c,d], Shachin Patra[a], Dennis R. Winge[b,e], Catherine L. Drennan[c,d,f], Jared Rutter[b,g] and David P. Barondeau[a]

[a]Department of Chemistry, Texas A&M University, College Station, TX 77842.

[b]Department of Biochemistry, University of Utah School of Medicine, Salt Lake City, UT 84112.

[c]Department of Biology, Massachusetts Institute of Technology, Cambridge, Massachusetts 02139.

[d]Howard Hughes Medical Institute, Massachusetts Institute of Technology, Cambridge, Massachusetts 02139.

[e]Department of Medicine, University of Utah School of Medicine, Salt Lake City, Utah 84132.

[f]Department of Chemistry, Massachusetts Institute of Technology, Cambridge, Massachusetts 02139.

[g]Howard Hughes Medical Institute, University of Utah School of Medicine, Salt Lake City, Utah 84132.

Table S1. Crystallographic data collection and refinement statistics.

	NFS1-ISD11-ACP$_{ec}$ (Se-met)[a]	**NFS1-ISD11-ACP$_{ec}$ (Native)**
PDB code		5USR
Data collection	SSRL 7-1	SSRL 7-1
Space group	$P2_12_12_1$	$P2_12_12_1$
Cell dimensions		
a, b, c (Å)	125.53, 147.69, 168.09	125.48, 147.78, 168.45
α, β, γ (°)	90, 90, 90	90, 90, 90
Wavelength (Å)	0.9776	1.12709
Resolution (Å)[b]	50.00 - 3.68 (3.74 - 3.68)	50.00 - 3.09 (3.14 - 3.09)
R_{sym} (%)[b]	14.1 (>100)[c]	6.7 (>100)[c]
R_{meas} (%)[b]	14.4 (>100)[c]	6.9 (>100)[c]
$CC_{1/2}$ (%)[b,d]	N.A. (85.7)	N.A. (61.9)
$<I/\sigma(I)>$[b]	39 (3.4)	40 (2.0)
Completeness (%)[b]	99.9 (99.0)	99.4 (88.6)
Redundancy[b]	28.9 (26.9)	8.0 (7.4)
Refinement		
Resolution (Å)		47.83-3.09
Total reflections		58013
R_{work}/R_{free}		0.212/0.259
No. atoms		
all		15666
N'-pyridoxyl-lysine-5'-monophosphate (LLP)		96
S-dodecanoyl-4'-phosphopantetheine (8Q1)		136
B-factors		
average		127.2
LLP		107.7
8Q1		109.3
R.m.s deviations		
Bond lengths (Å)		0.002
Bond angles (°)		0.547
Ramachandran outliers (%)		
Favored		95.2
Outliers		0.4
Rotamer outliers (%)		1.2
Clash Score		7.2

[a]Bijvoet pairs were kept separate during data processing.

[b]Values in parentheses reflect the highest resolution bin.

[c]Values greater than 100% were reported as 0.000 by version of HKL2000/Scalepack.

[d]Average $CC_{1/2}$ was not reported by version of HKL2000/Scalepack.

Table S2. Residues modeled in the X-ray crystal structure of SDA_{ec}.

Chain	Protein	SDA_{ec} residues	Residues not modeled	Average B-factor (Å^2)
A	NFS1	56-457	283-293, 368-384, 446-457	112.2
B	ISD11	1-91	1-3, 80-91	110.4
C	NFS1	56-457	87-95, 283-294, 373-388, 445-457	149.7
D	ISD11	1-91	1-3, 84-91	113.5
E	NFS1	56-457	87-94, 276-294, 360-401,437-457	99.1
F	ISD11	1-91	1-3, 79-91	97.1
G	NFS1	56-457	61-65, 87-97, 276-294, 367-402, 441-457	111.7
H	ISD11	1-91	1-2, 80-91	110.9
I	ACP_{ec}	1-78	1, 78	153.6
J	ACP_{ec}	1-78	1-2, 78	193.7
K	ACP_{ec}	1-78	1-4, 74-78	202.4
L	ACP_{ec}	1-78	1-2, 74-78	211.1

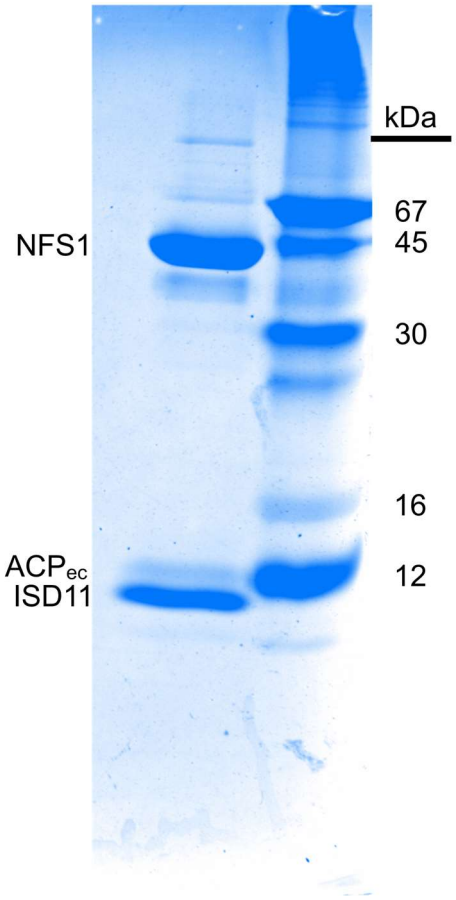

Figure S1. Human NFS1-ISD11 co-purifies with *E. coli* ACP. A 14% SDS-PAGE gel shows the presence of NFS1, ISD11, and *E. coli* ACP (ACP_{ec}). ACP_{ec} (apo-MW = 8.6 kDa with pI = 4, 4'-PPT MW = 358 Da) stains poorly with Coomassie Blue and migrates to a position larger than its predicted molecular weight.

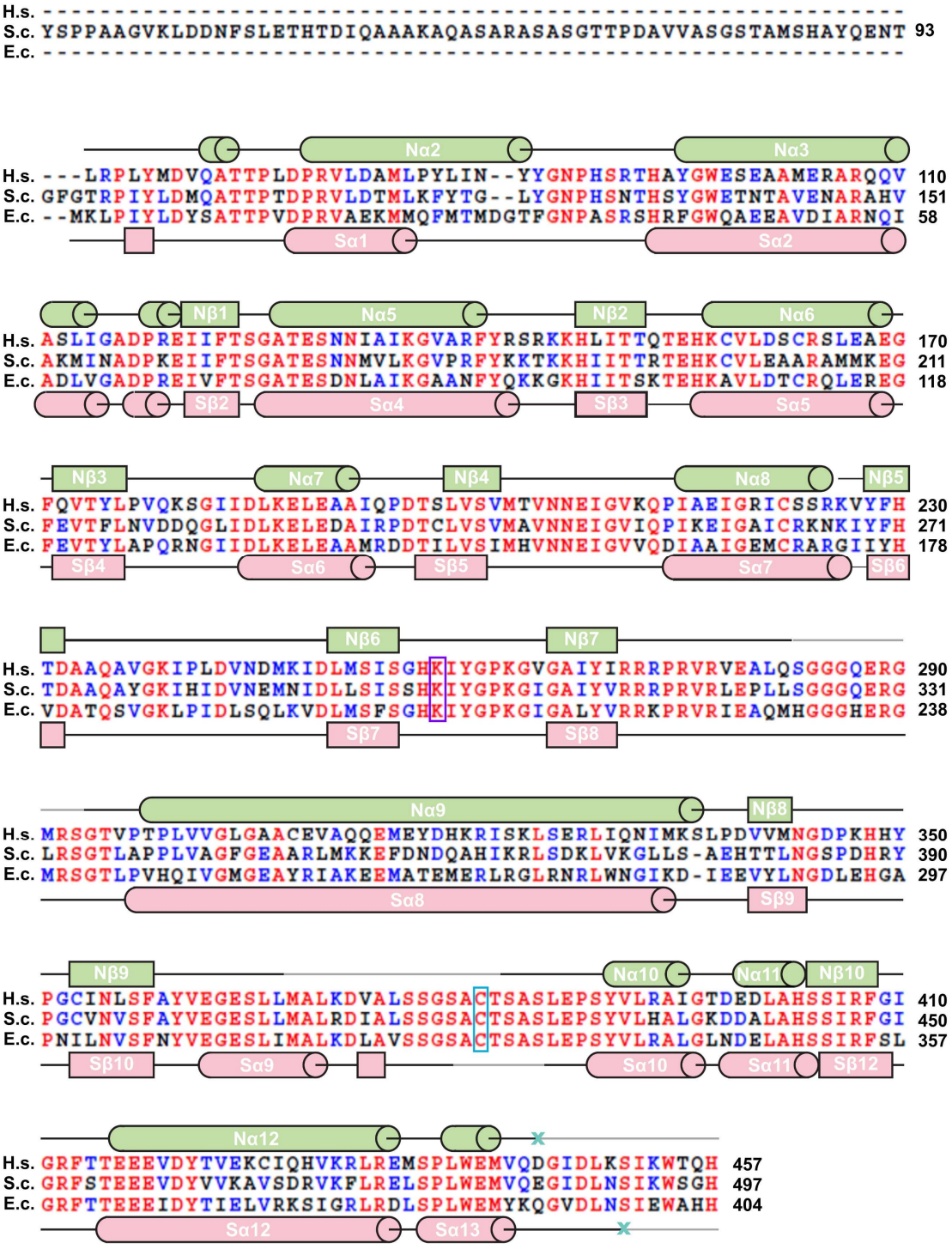

Figure S2. Secondary structure and sequence alignment for NFS1. Aligned sequences are displayed for *Homo sapiens* (H.s.) NFS1, *S. cerevisiae* (S.c.) Nfs1, and *E. coli* (E.c.) IscS. Secondary structure elements for NFS1 (light green) were determined by removing helix and sheet records provided by Phenix and allowing Pymol to provide the assignment. Secondary structure elements for IscS (light pink) were assigned based on the PDB header. Blue X's indicate the position of the last residues built into the most complete chain for the NFS1 and IscS (PDB code: 3LVM) structures. Light grey sections between secondary structure elements indicate disordered regions. The Lys that covalently attached to the PLP (K258 in NFS1) and the Cys in the mobile S-loop (C381 in NFS1) are highlighted in violet and sky blue boxes, respectively. Amino acid labels in red are fully conserved, while those in blue are conserved in at least 50% of the compared organisms.

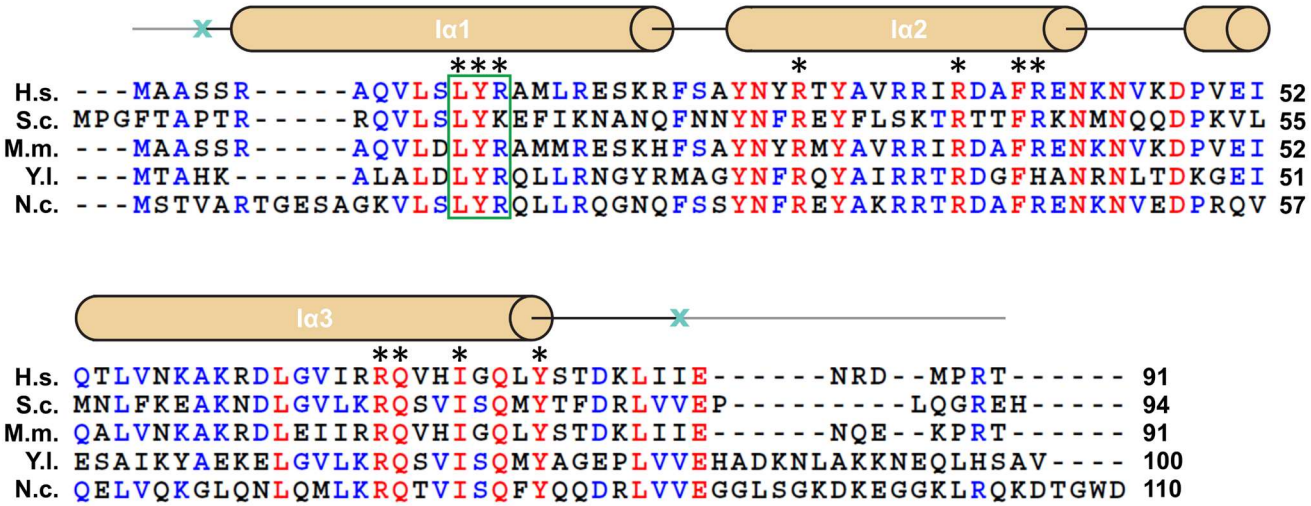

Figure S3. Secondary structure and sequence alignment for ISD11. Secondary structure elements for ISD11 were mapped (similar to Fig. S2) to a sequence alignment containing *H. sapiens* (H.s.), *S. cerevisiae* (S.c.), *Mus musculus* (M.m.), *Yarrowia lipolytica* (Y.l.), and *Neurospora crassa* (N.c.). Asterisks indicate residues targeted by mutagenesis studies. The LYR-motif is highlighted with a green box. Blue X's indicate the position of the last residues built into the most complete chain for ISD11. Amino acid labels indicate conservation level (red is fully conserved, blue is >50% conserved).

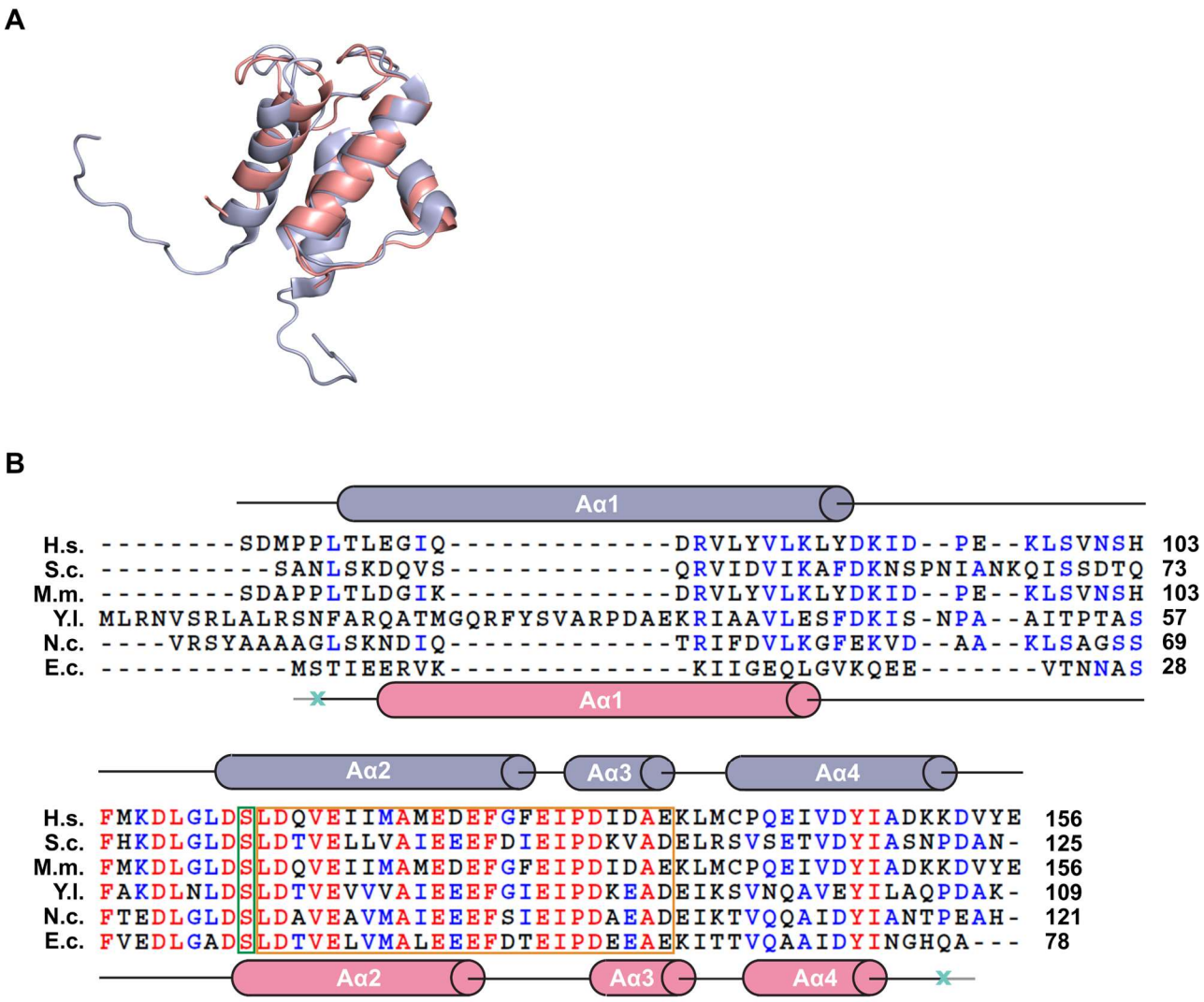

Figure S4. Structural and sequence comparison of ACP_{ec} with eukaryotic homologs. (*A*) Structural overlay of ACP_{ec} (chain L, salmon) with human mitochondrial ACP (plum; PDB code: 2DNW), which have a Cα rmsd of 1.3 Å for 66 atoms. (*B*) Secondary structures for human and *E. coli* ACP were mapped to sequence alignments similar to Figs. S2 and S3. The conserved serine that covalently attaches to the 4'-PPT is highlighted with a green box, and the ISD11 interacting region is highlighted with an orange box. Blue X's indicate the position of the last residues built into the most complete chain for ACP_{ec}. Amino acid labels show conservation level (red is fully conserved, blue is >50% conserved).

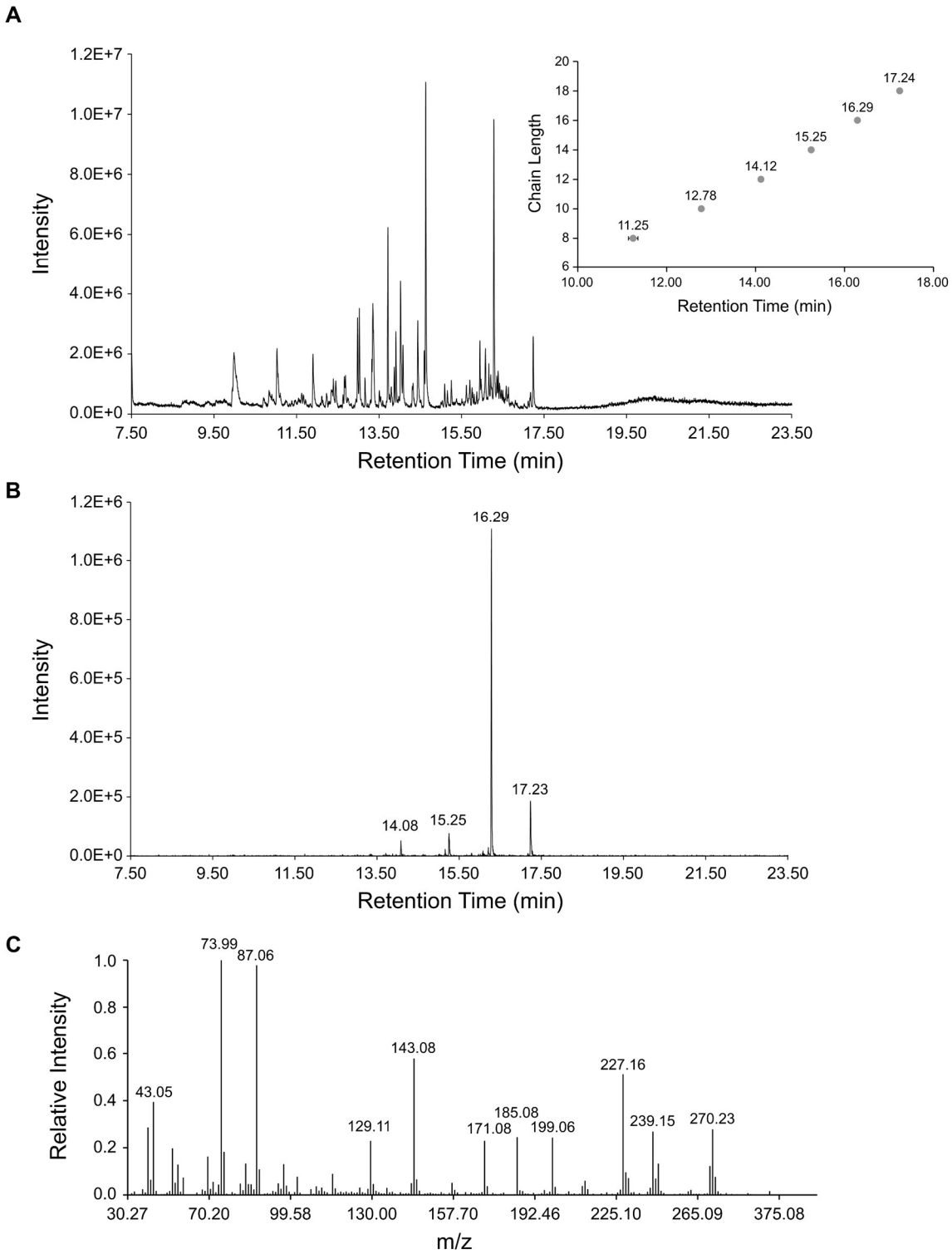

Figure S5. Identification of 4'-PPT conjugated fatty acids associated with the SDA_{ec} complex. (*A*) Representative raw total ion chromatogram (TIC) for isolated FAMEs from a transesterified sample of SDA_{ec}. Inset displays the retention time of standard FAMEs (n = 2). (*B*) Representative TIC filtered by m/z = 73.5-74.5, a high probability fragment from electron ionization (EI) of FAMEs. (*C*) A representative EI fragmentation pattern of the peak at t = 16.29 min (corresponding to a chain length of 16 carbons). Analysis of unknown transesterified SDA_{ec} samples were conducted in triplicate.

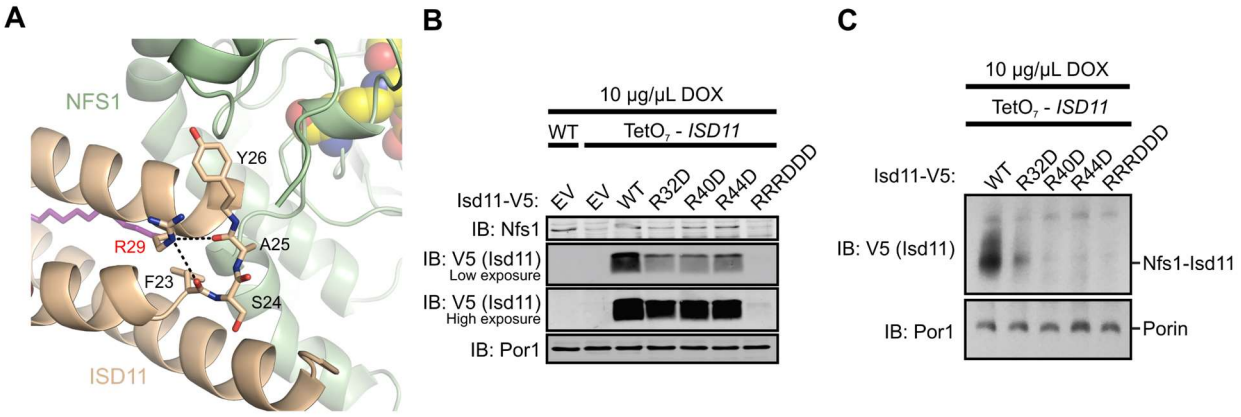

Figure S6. Arg residues are important for ISD11 stability and interactions with $ACP_{ec.}$ (*A*) R29 forms hydrogen bonds to the backbone carbonyl oxygen atoms of the F23-containing loop. NFS1 and ISD11 are displayed in light green and wheat, respectively. The PLP is displayed as spheres and the acyl-chain is shown in purple. Residues targeted by mutagenesis experiments are highlighted in red. Purified mitochondria from the indicated *S. cerevisiae* strains were either resolved by SDS-PAGE (*B*) or solubilized in 1% digitonin and resolved by BN-PAGE (*C*). Cells were grown for 18 h in the presence 10 µg/mL doxycycline. The indicated proteins and protein complexes were assessed by immunoblot. The R32D R40D R44D variant (equivalent to human R29D R37D R41D) is labeled RRRDDD.

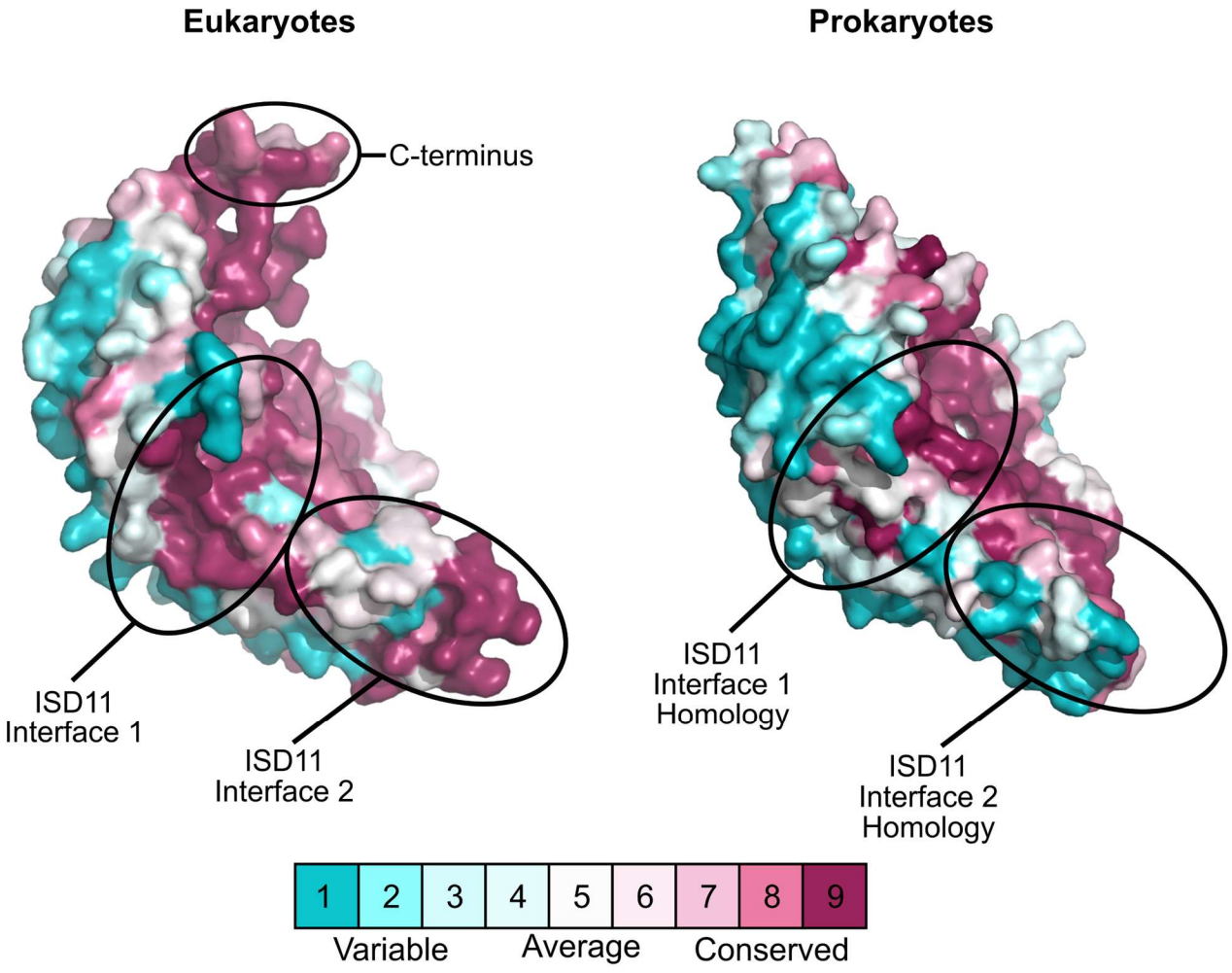

Figure S7. Eukaryotic cysteine desulfurases have conserved interfaces for binding ISD11. Eukaryotic (n = 64) and prokaryotic (n = 45) group I cysteine desulfurase sequences were aligned separately and sequence conservation was mapped onto NFS1 for eukaryotes and onto IscS (PDB code: 3LVM) for prokaryotes. The C-terminal region of NFS1, which likely interacts with ISCU2, is also highly conserved. The equivalent highly conserved C-terminal region for IscS is in a different conformation that is not visible in this orientation. Consurf scores, indicating relative conservation, are displayed in the scale bar.

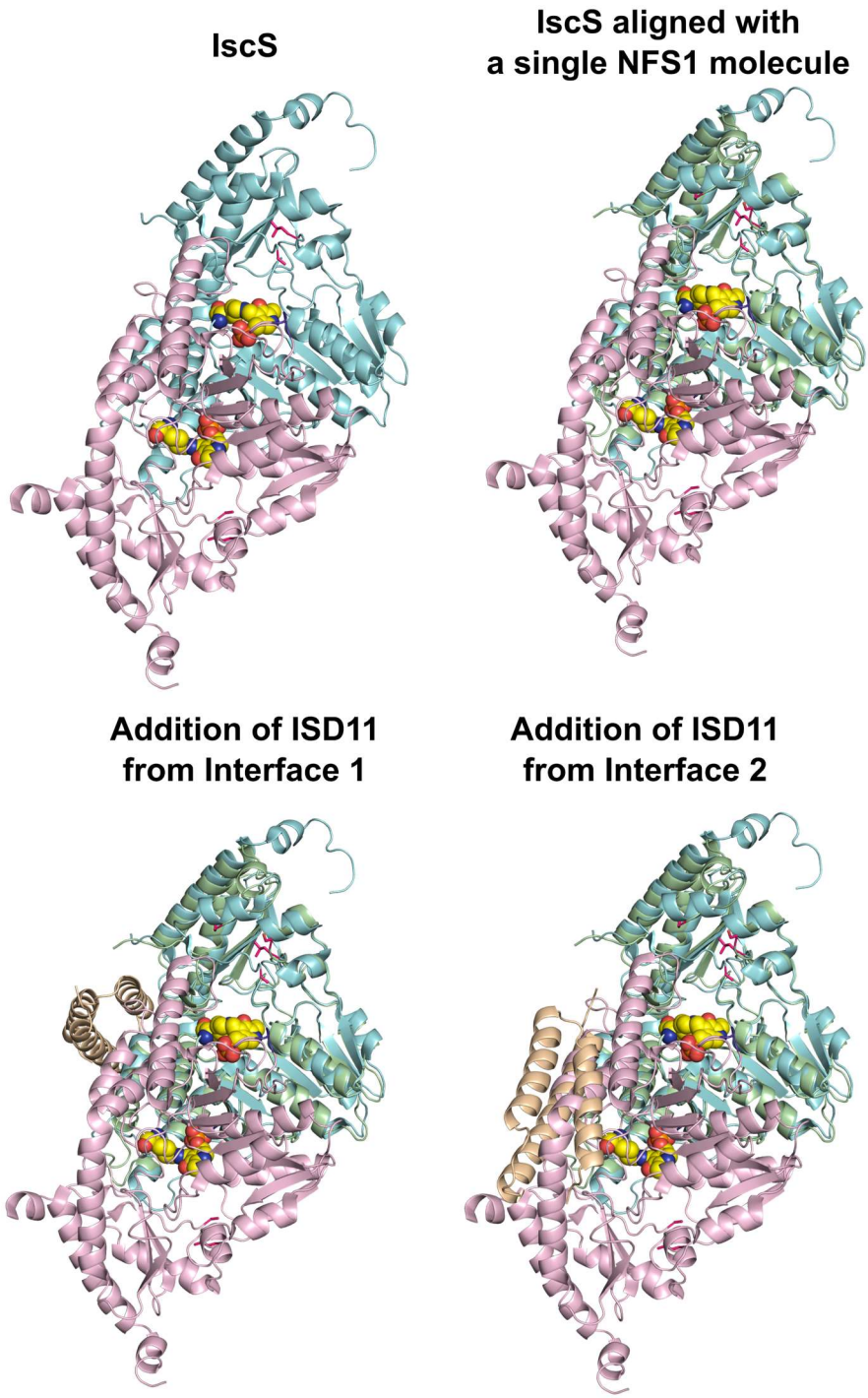

Figure S8. IscS and NFS1 have different quaternary structures. Ribbon diagram for the IscS structure (top left, PDB code: 3LVM) with subunits displayed in pink and cyan. The PLP cofactors are displayed as spheres. NFS1 (green) aligned with the cyan subunit of IscS is shown on the top right. ISD11 (wheat) added to NFS1 interface 1 does not overlap with IscS (bottom left). In contrast, the addition of ISD11 to NFS1 interface 2 is sterically precluded by the second subunit (pink) of the IscS dimer (bottom right).

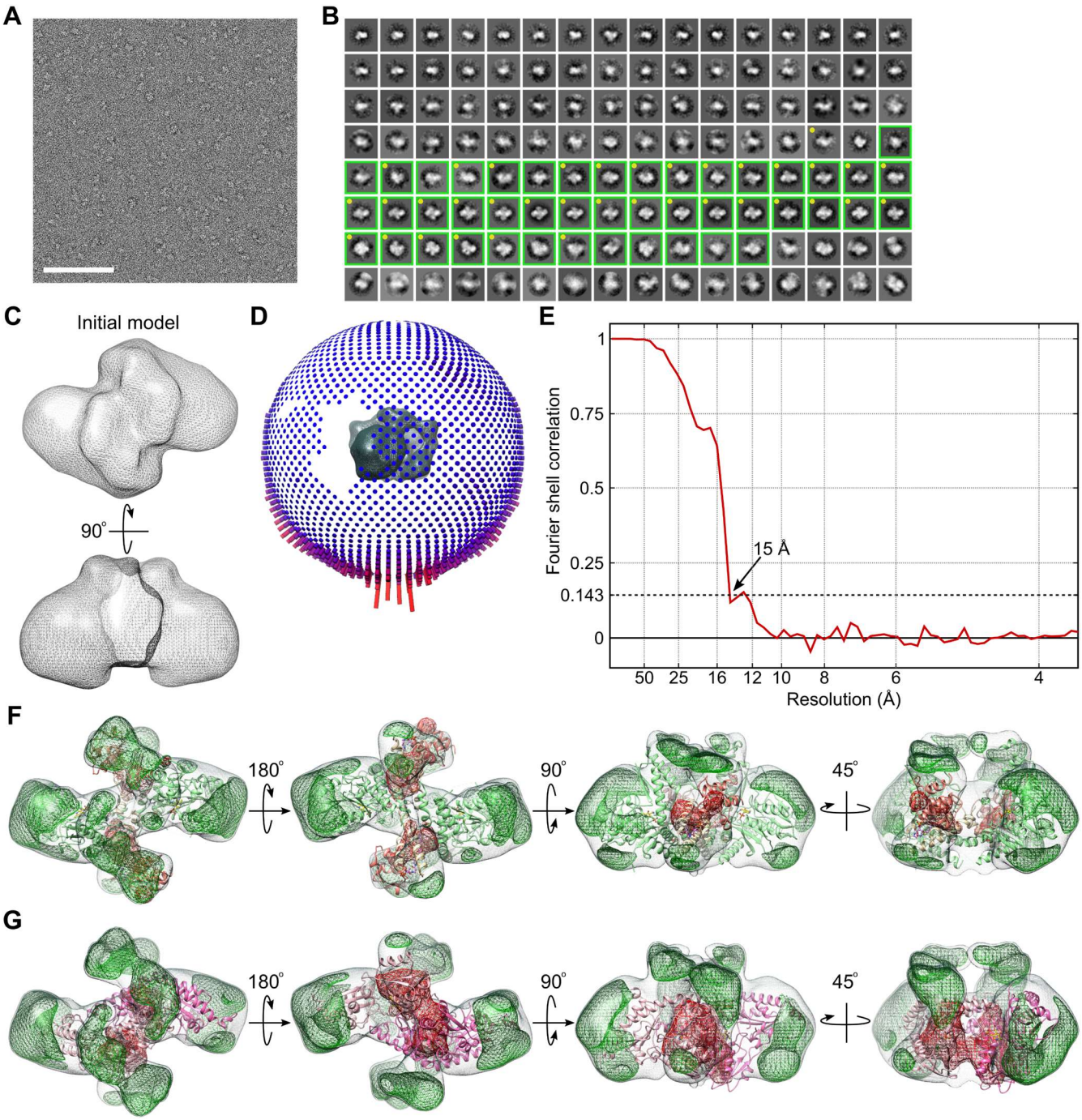

Figure S9. EM images of a negative stained specimen of SDA_{ec} were of sufficient quality to produce a reliable 3D reconstruction of the complex. (*A*) A representative area from a micrograph showing suitable particle distribution and contrast of the negative stained specimen. Scale bar represents 100 nm. (*B*) 2D class averages from all windowed particles. Each average panel is 235 Å wide. Comprised of more than half of the total windowed particles, the 45 well-defined classes that were retained for further image analysis are highlighted in green. (*C*) Initial model (isosurface contoured with gray mesh) generated from a subset of the class averages marked with yellow dots in panel B. (*D*) Particles show a preferred orientation but are sufficiently distributed to produce a complete reconstruction. Height and color of the bars indicates number of particles assigned to a particular view relative to reconstruction (dark gray mesh, also shown in Fig. 4). (*E*) Plot of Fourier shell correlation (FSC) between reconstructions that were calculated from independently refined half-sets of particles suggests a nominal resolution of approximately 15 Å. (*F*) Difference maps (positive in green mesh, negative in red mesh) calculated by subtracting the fit SDA_{ec} structure (subunits colored as in Fig. 1) from the EM density map (gray transparent mesh). (*G*) Difference maps after subtracting the fit *E. coli* IscS (PDB code: 3LVM) from the EM map. Note the substantial negative difference density in the center of the IscS dimer indicating a poor match with the EM density, whereas the SDA_{ec} has only minor patches of negative density.

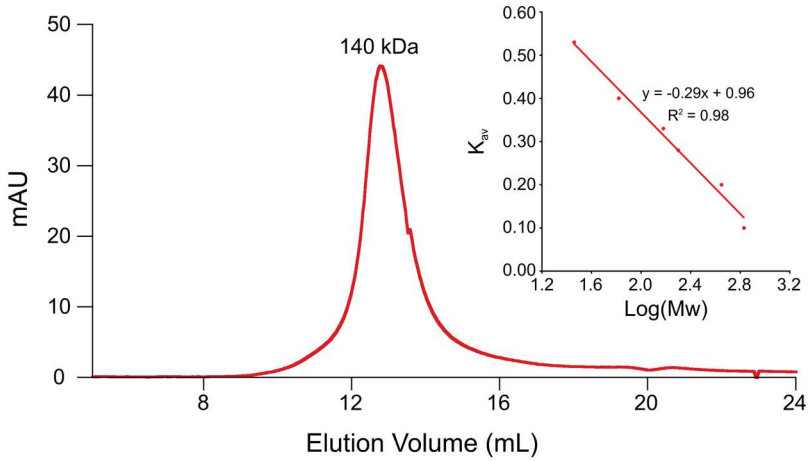

Figure S10. The SDA_{ec} complex is a dimer in solution. Representative data for S200 size exclusion analysis of the SDA_{ec} complex (10 µM, 500 µL injection). Inset shows the average K_{av} for standards (thyroglobulin 669 kDa, apoferritin 443 kDa, β-amylase 200 kDa, alcohol dehydrogenase 150 kDa, albumin 66 kDa, carbonic anhydrase 29 kDa) run in triplicate. Duplicate runs of blue dextran were used to determine the void volume.

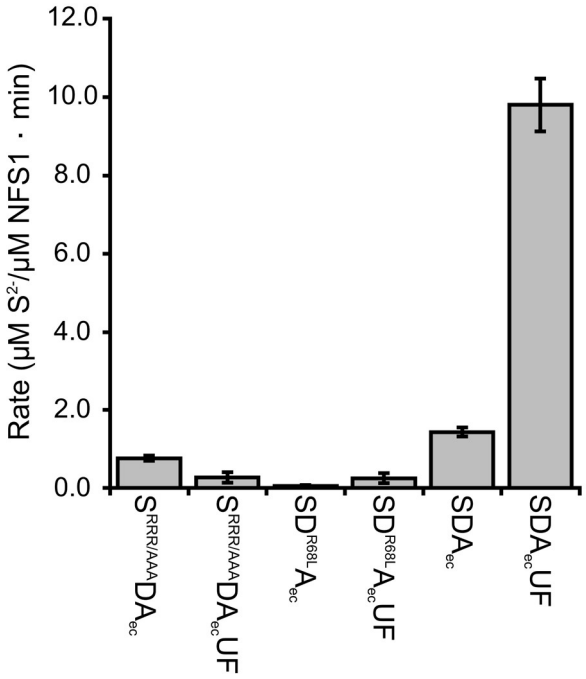

Figure S11. NFS1-ISD11 variants result in the loss of FXN-based stimulation for the cysteine desulfurase activity. The methylene blue assay was conducted for cysteine desulfurase activity in the presence of 100 μM cysteine, 0.5 μM SDA_{ec} (or corresponding variant), 4 mM D, L-DTT, 10 μM PLP, and 1.5 μM ISCU2 and FXN (when included). Reactions were quenched after 6 min, sulfide was quantified, and initial rates were determined. Standard deviations represent the error in triplicate measurement. SDA_{ec}UF corresponds to the SDA_{ec} complex that also includes ISCU2 and FXN.

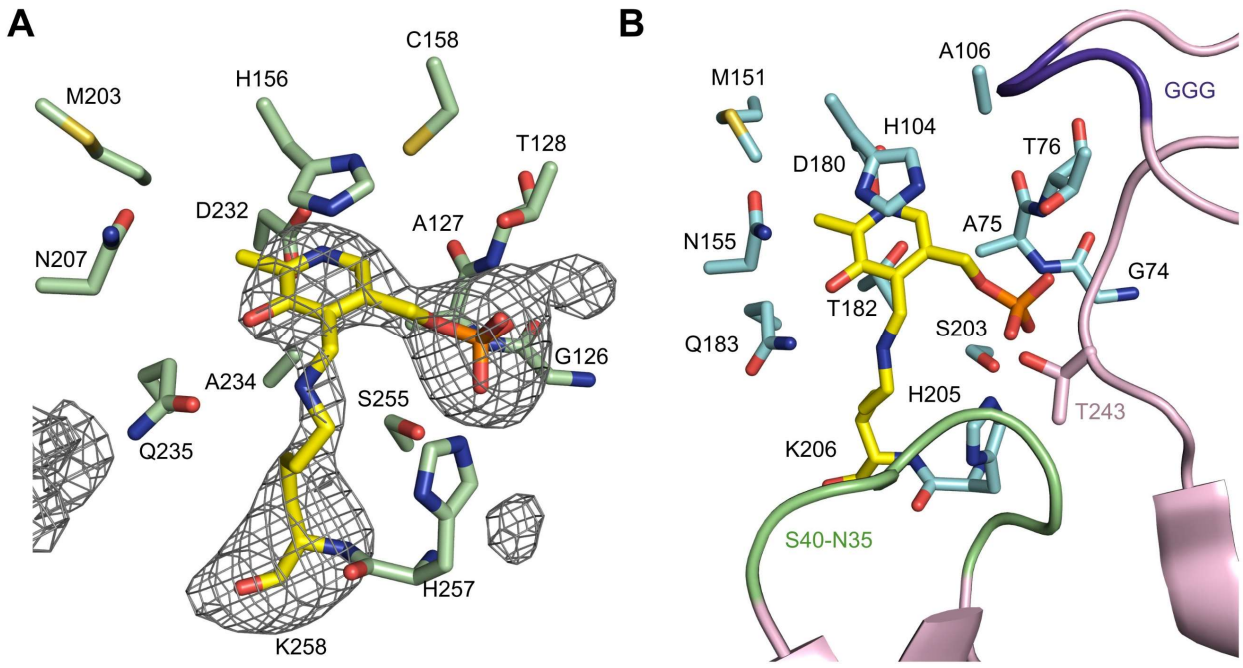

Figure S12. Comparison of the active sites for NFS1 and IscS. The NFS1 (A) and IscS (B) active sites displayed in a similar orientation reveals comparable intrasubunit interactions with the PLP. Intersubunit interactions (S40-N35 loop, green; GGG motif purple, other residues from second subunit including T243, magenta) also contribute to the active site for IscS (PDB code: 3LVM) that are not present in NFS1. Simulated annealing - omit mF_o-DF_c map contoured to 3.0σ (grey mesh) is shown for the PLP-K258 of NFS1. The map was displayed with a 5 Å region padding.

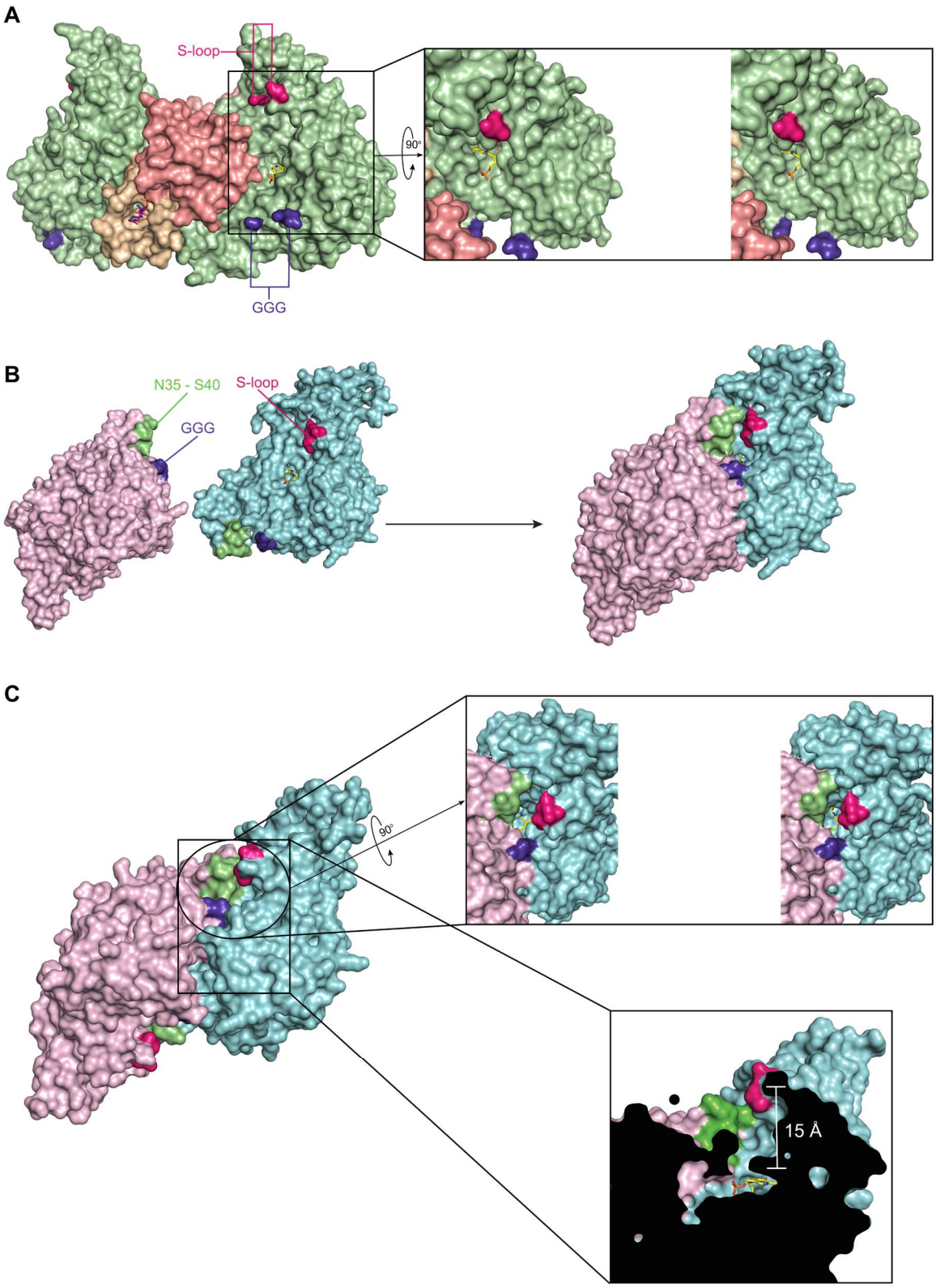

Figure S13. The PLP is solvent exposed in the SDA_{ec} complex and buried in the IscS structure. (*A*) Surface view of NFS1 active site reveals that it is shallow and solvent exposed. Inset shows a stereo view of the active site with the PLP (yellow). (*B*) The formation of the IscS dimer buries the PLP between the monomeric units. (*C*) Stereo view of the IscS substrate tunnel (top right), and a surface clip of the dimer interface displaying the depth of the substrate tunnel (bottom right).

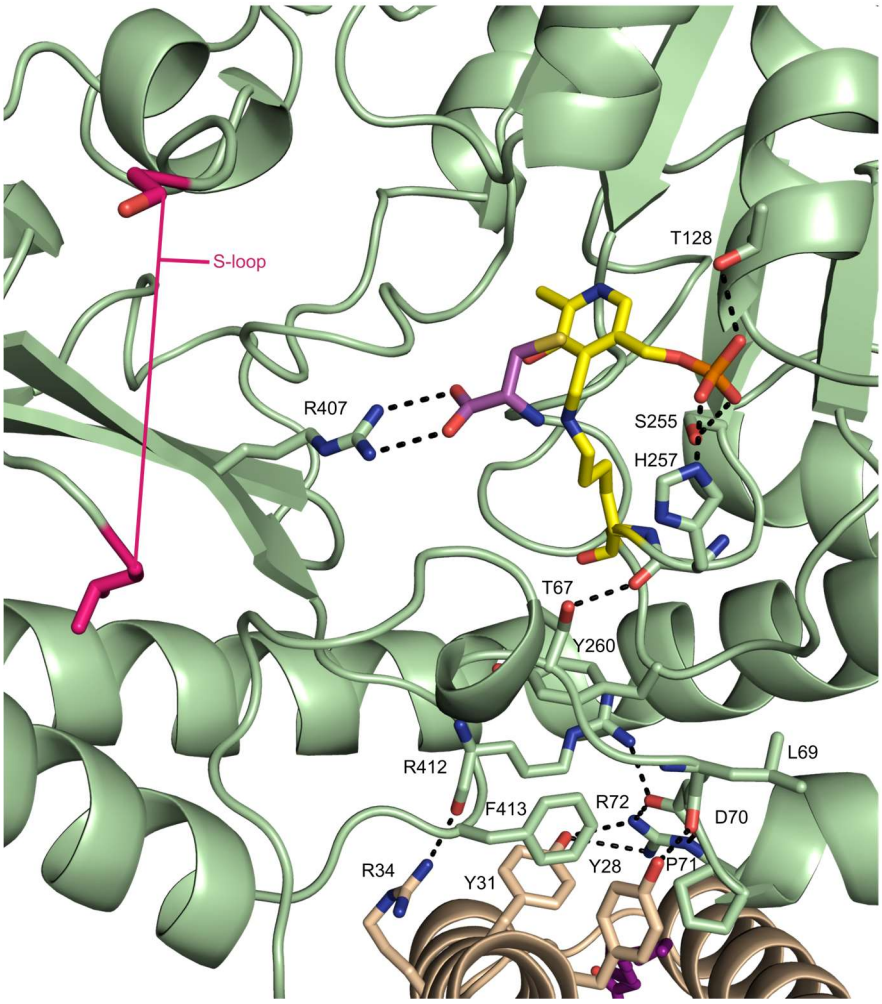

Figure S14. Hydrogen bonding network between the acyl-chain and PLP active site for the SDA_{ec} complex. Conserved residues on NFS1 provide a relay of hydrogen bonds that propagate between the Lys-bound PLP cofactor (carbons in yellow) and the acyl-chain of the 4'-PPT (magenta). The cysteine substrate (carbons in magenta) was modeled into the active site based on a substrate bound SufS structure (PDB code: 5DB5). Residues connecting disordered mobile S-loop are shown in hot pink.

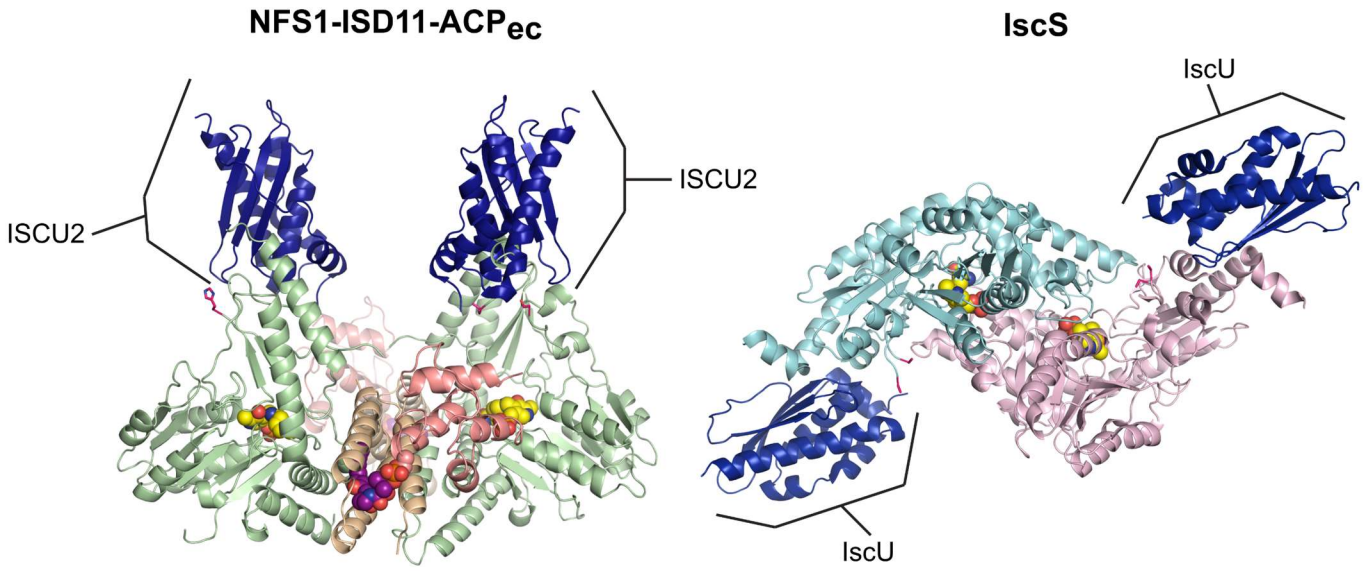

Figure S15. Modeling suggests the relative positions of the scaffold subunits are different in the NFS1-ISD11-ACP_{ec}-ISCU2 and IscS-IscU structures. The interactions between the NFS1 subunit of the SDA_{ec} complex and ISCU2 were modeled (left) based on the analogous interactions in the IscS-IscU structure (PDB code: 3LVL, right).

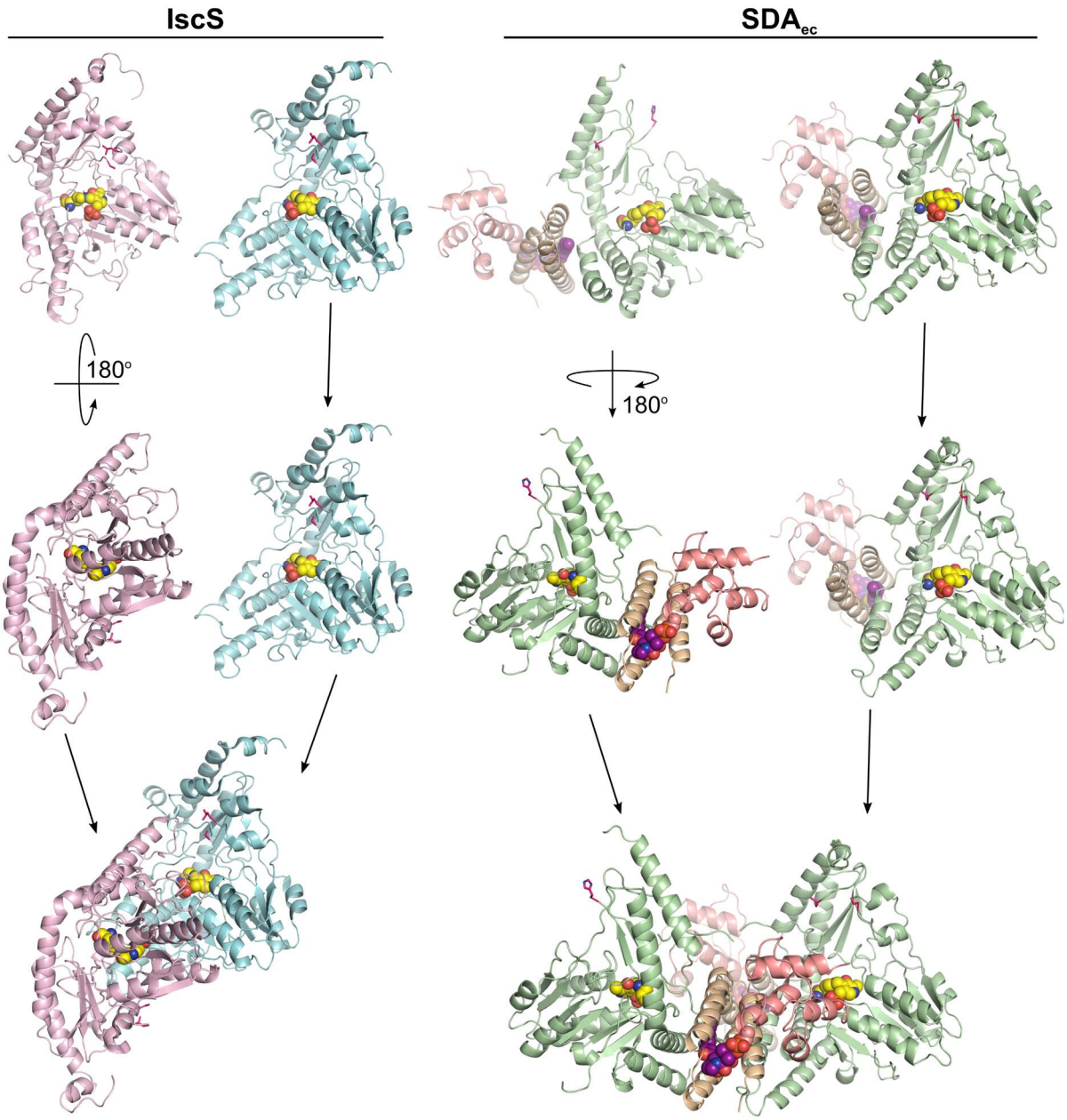

Figure S16. Proposed assembly pathways for generation of the IscS and NFS1-ISD11-ACP$_{ec}$ architectures. IscS (PDB code: 3LVM) assembles as a tight homodimer (left). NFS1-ISD11-ACP$_{ec}$ assembles via a monomeric pathway utilizing two NFS1-ISD11-ACP$_{ec}$ units to produce the final complex (right).

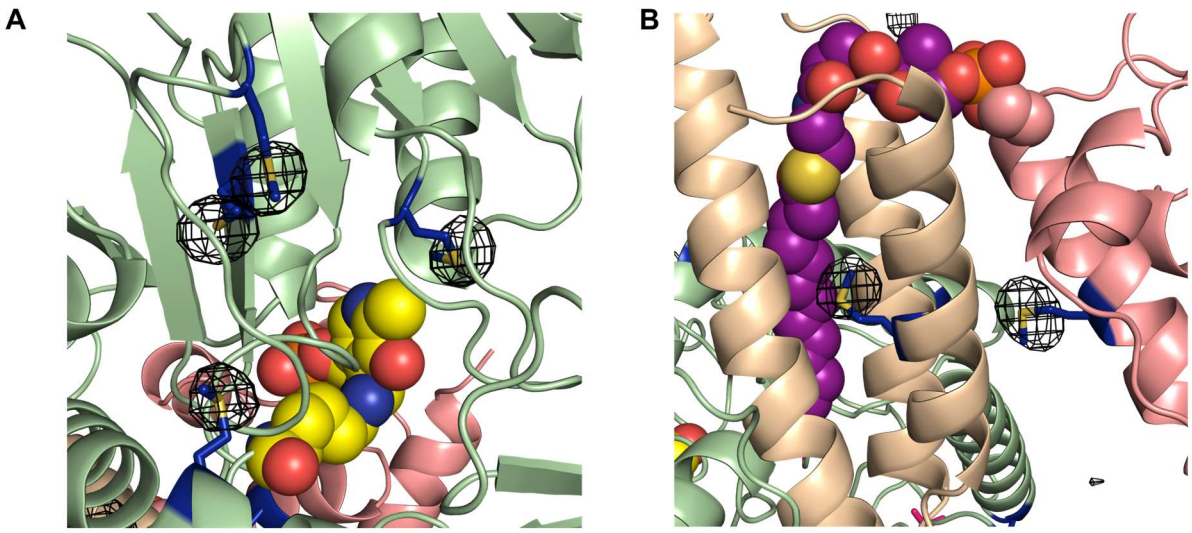

Figure S17. Anomalous data identifies positions of selenium atoms in the structure of NFS1. Regions near the (A) PLP (yellow spheres) and (B) 4'-PPT (purple spheres) are displayed for the SDA_{ec} complex. Ribbon diagrams for NFS1 (light green), ISD11 (wheat), and ACP_{ec} (salmon) are displayed with anomalous difference electron density contoured at 6.0σ (black mesh).